Numerical modeling of steel deck slabs with position based finite element method and immersion techniques

Rodrigo S. Melo[1], Rogério Carrazedo[1], Chiara P. Teodoro[1]

[1]*Dept. of Structural Engineering, University of São Paulo*
Avenida Trabalhador São Carlense 400, 13566-590, São Paulo, Brazil
rodrigomelo@usp.br, rogcarrazedo@sc.usp.br, chiarapteodoro@usp.br

Abstract. Steel deck slabs are an efficient construction system thanks to the deck's double role of molding the concrete in the builiding phase and resisting to flexural loads within its lifespan. Due to the high costs and semiempirical nature of experimental programs, it is important to formulate a numerical model that accurately describes the behavior of these structures. This article proposes a simple and computationally lightweight numerical model employing a finite element method based on positions, which naturally allows for geometrical nonlinear analysis of structures. A prismatic element is developed to represent the concrete matrix, and active face immersed elements are included to represent the steel deck. The results are expected to conform with previous experimental results from literature under the limitations of the employed simplifications.

Keywords: Steel deck slabs, Finite element method, Immersion techniques

1 Introduction

Concrete and steel are one of the most popular material combinations for construction, thanks to concrete's low cost and high compressive strength and steel's high tensile strength and lightweightness. Reinforced concrete structures aside, this pair can be seen in steel framed buildings in the form of steel deck slabs. In these, concrete is poured over a continuous steel deck placed between two spans to form a composite one-way slab. The deck functions both as formwork for the poured concrete during construction and as flexural reinforcement in the lifespan of the structure.

To understand the behavior and performance of steel deck slabs, many experimental tests have been performed and reported in literature, such as [1], [2]. Due to the costly nature of experimental research, it is of interest to formulate numerical models to reproduce and predict the behavior of these structures, as done by [3], [4].

The present work proposes a simplified numerical modeling of steel deck slabs in which slipping is not considered. While it has been demonstrated that the slipping is an important factor to consider in these systems when physical nonlinearities start to become prominent ([1], [2], [4]), it is valuable to be able to numerically reproduce the linear behavior of these systems with less computationally costly simulations.

The modeling is done via finite element method (FEM) based on positions, which is an approach initially proposed by Bonet et al. [5] and independently by Coda and Greco [6] that naturally encompasses geometrical nonlinearity. Triangular base prismatic elements work as the concrete matrix and the steel decking is represented by active face immersed elements proposed by Carrazedo et al. [7]. The procedure involves first calculating rectangular bidimensional elements representing the steel. Their stiffness is then made to contribute to the faces of the prismatic matrix elements where the steel decking is located. This way, no new degrees of freedom are effectively added to the problem, considerably reducing the computational cost of simulations.

2 FEM based on positions

The main principle of the FEM based on positions is to use coordinates rather than displacements as variables. To start, an element is described as shown in Fig. 1 in its initial configuration B_0 with coordinates x_i and in its current configuration B_1 with coordinates y_i, with $i = 1, 2$ for 2D spaces or $i = 1, 2, 3$ for 3D spaces. A third adimensional description in coordinates ξ_i is made to facilitate numerical calculations and to help transit between the two real configurations.

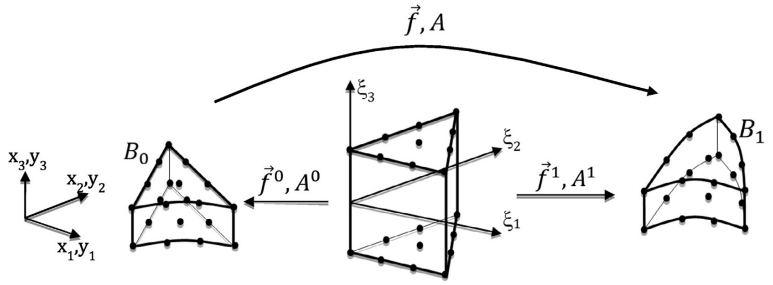

Figure 1. Element mapping

The change of configuration function $\vec{f}$ is one that takes the coordinates of the body from its initial to its current configuration. It can be split into a composition of the functions $\vec{f}^0$ and $\vec{f}^1$ which take an adimensional element to the body's initial and final configurations respectively. Note that these functions are effectively the body coordinates themselves, that is, $f_i^0(\xi_j) = x_i$ and $f_i^1(\xi_j) = y_i$.

The gradient of $\vec{f}$, defined as $\boldsymbol{A}$ and often denoted deformation gradient, can similarly be described by a combination of $\boldsymbol{A^0}$ and $\boldsymbol{A^1}$ which are the gradients of $\vec{f}^0$ and $\vec{f}^1$ respectively. Those entities are defined by

$$A_{ij}^0 = \frac{\partial x_i}{\partial \xi_j}, \tag{1}$$

$$A_{ij}^1 = \frac{\partial y_i}{\partial \xi_j}. \tag{2}$$

With these, $\boldsymbol{A}$ can be written as

$$\boldsymbol{A} = (\boldsymbol{A^0})^{-1}\boldsymbol{A^1}. \tag{3}$$

The deformation gradient can then be used to work out the Green-Lagrange strain, which is defined by

$$\boldsymbol{L} = \frac{1}{2}(\boldsymbol{A}^T\boldsymbol{A} - \boldsymbol{I}), \tag{4}$$

where $\boldsymbol{I}$ is the identity tensor.

To work out stresses from strains, the Saint-Venant-Kirchhoff (SVK) constitutive relation is adopted. It is written as a linear relation between the Green-Lagrange strain and its energetically conjugate Piola-Kirchhoff stress. It follows that the strain energy per unit of volume in the SVK model is defined as

$$u_e = \frac{1}{2}\boldsymbol{L} : \mathfrak{C} : \boldsymbol{L}. \tag{5}$$

The Piola-Kirchhoff stress can then be written as

$$\boldsymbol{S} = \frac{\partial u_e}{\partial \boldsymbol{L}} = \mathfrak{C} : \boldsymbol{L}, \tag{6}$$

where $\mathfrak{C}$ is the constitutive fourth-order tensor that encompasses the material properties. For isotropic materials, this tensor can be written in Voigt notation as

$$\begin{Bmatrix} S_{11} \\ S_{22} \\ S_{33} \\ S_{23} \\ S_{13} \\ S_{12} \end{Bmatrix} = \frac{E}{(1+\nu)(1-2\nu)} \begin{bmatrix} 1-\nu & \nu & \nu & 0 & 0 & 0 \\ \nu & 1-\nu & \nu & 0 & 0 & 0 \\ \nu & \nu & 1-\nu & 0 & 0 & 0 \\ 0 & 0 & 0 & 1-2\nu & 0 & 0 \\ 0 & 0 & 0 & 0 & 1-2\nu & 0 \\ 0 & 0 & 0 & 0 & 0 & 1-2\nu \end{bmatrix} \begin{Bmatrix} L_{11} \\ L_{22} \\ L_{33} \\ L_{23} \\ L_{13} \\ L_{12} \end{Bmatrix}. \tag{7}$$

With those quantities defined, the total potential energy of the element can be described in two parts. The energy related to nodal applied forces is given by

$$\mathbb{P} = -\vec{F} \cdot \vec{Y}, \tag{8}$$

where $\vec{F}$ holds the values of the applied forces and $\vec{Y}$ contains the node positions of the body in its current configuration. It is important to note that in this formulation the applied forces are considered to be conservative, that is, independent of the current position.

The strain energy of the body is given by

$$\mathbb{U} = \int_{V_0} u_e \, dV. \tag{9}$$

With eq. (5), the derivative of the strain energy with relation to current position $\vec{Y}$ can be worked out as

$$\frac{\partial \mathbb{U}}{\partial \vec{Y}} = \int_{V_0} \frac{\partial u_e}{\partial \vec{Y}} \, dV = \int_{V_0} \frac{\partial u_e}{\partial \boldsymbol{L}} : \frac{\partial \boldsymbol{L}}{\partial \vec{Y}} \, dV = \int_{V_0} \boldsymbol{S} : \frac{\partial \boldsymbol{L}}{\partial \vec{Y}} \, dV. \tag{10}$$

The total potential energy can finally be written as

$$\Pi = \mathbb{P} + \mathbb{U}. \tag{11}$$

In the equilibrium position, it is known by principle that the total energy is stationary. Thus, if the nodal position is chosen as the main variable, the total energy variation in the equilibrium position can be written as

$$\delta\Pi = \frac{\partial \Pi}{\partial \vec{Y}} \delta\vec{Y} = \frac{\partial \mathbb{P}}{\partial \vec{Y}} \delta\vec{Y} + \frac{\partial \mathbb{U}}{\partial \vec{Y}} \delta\vec{Y} = \vec{0} \tag{12}$$

Since $\delta\vec{Y}$ can be chosen arbitrarily, it follows that $\delta\Pi/\delta\vec{Y}$ must be zero. From that and eqs. (8) and (10), the equilibrium of external and internal forces is worked out to be

$$-\vec{F} + \int_{V_0} \boldsymbol{S} : \frac{\partial \boldsymbol{L}}{\partial \vec{Y}} \, dV = \vec{0}. \tag{13}$$

In the system of equations above, $\vec{F}$ is given and $\boldsymbol{L}$ and $\boldsymbol{S}$ are nonlinearly dependent to the vector of unknowns $\vec{Y}$. An approximate solution can be found via an iteractive procedure called the Newton-Raphson method. It begins by assigning to eq. (13) trial position $\vec{Y}^*$ which can initially be made equal to the initial node positions $\vec{X}$. As $\vec{Y}^*$ is not the actual solution, eq. (13) is not equal to zero but to a vector $\vec{g}$, denoted mechanical unbalanced force, as seen below:

$$\vec{g}(\vec{Y}^*) = -\vec{F} + \int_{V_0} \boldsymbol{S}(\vec{Y}^*) : \frac{\partial \boldsymbol{L}}{\partial \vec{Y}}\Big|_{\vec{Y}^*} \, dV. \tag{14}$$

This vector is then expanded around the equilibrium position where it should be equal to zero. By ignoring higher order terms, the following equality is imposed:

$$\vec{g}(\vec{Y}) = \vec{g}(\vec{Y}^*) + \frac{\partial \vec{g}}{\partial \vec{Y}}\Big|_{\vec{Y}^*} \Delta\vec{Y} = \vec{0} \tag{15}$$

In the equation above, $\partial\vec{g}/\partial\vec{Y}$ is called Hessian matrix and $\Delta\vec{Y}$ is the position correction, which is the vector of unknowns of a now linear system of equations. The Hessian matrix is explicitly

$$\boldsymbol{H} = \frac{\partial \vec{g}}{\partial \vec{Y}} = \int_{V_0} \left(\frac{\partial \boldsymbol{S}}{\partial \vec{Y}} : \frac{\partial \boldsymbol{L}}{\partial \vec{Y}} + \boldsymbol{S} : \frac{\partial^2 \boldsymbol{L}}{\partial \vec{Y} \otimes \partial \vec{Y}} \right) dV \tag{16}$$

Once the linear system is solved for $\Delta\vec{Y}$, the trial position is updated in the following way:

$$\vec{Y}^* \leftarrow \vec{Y}^* + \Delta\vec{Y} \tag{17}$$

The process is then repeated until $\Delta\vec{Y}$ is sufficiently small, which implies $\vec{Y}^*$ is sufficiently close to $\vec{Y}$. This is generally determined by setting an upper threshold for the value of $||\Delta\vec{Y}||/||\vec{X}||$.

2.1 Triangular base prismatic element for the concrete matrix

Tridimensional, prismatic elements are picked to represent the concrete matrix. The base of the prism, described in the plane defined by directions ξ_1, ξ_2, is chosen to be triangular as that shape easily conforms to most cross section geometries. The degrees of approximation of the triangular base as well as the height are chosen to be cubic, which is achieved by distributing 10 nodes across the base and 4 groups of nodes across the height as shown in Fig. 2.

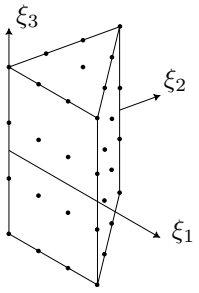

Figure 2. Prismatic element node distribution

Cubic complete polynomials are worked out in ξ_1, ξ_2 as the shape functions for the base and multiplied by third-order Lagrange polynomials in ξ_3 for a full description of the tridimensional geometry. The initial and current body coordinates can thus be expressed as

$$x_i = \phi_k(\xi_1, \xi_2, \xi_3) X_i^k \tag{18}$$

$$y_i = \phi_k(\xi_1, \xi_2, \xi_3) Y_i^k \tag{19}$$

where ϕ_k are the shape functions, $k = 1, \ldots, 40$, and X_i^k, Y_i^k are the coordinates of the k-th node.

With eqs. (18) and (19), eqs. (1) and (2) can be written as

$$A_{ij}^0 = \frac{\partial \phi_k}{\partial \xi_j} X_i^k \tag{20}$$

$$A_{ij}^1 = \frac{\partial \phi_k}{\partial \xi_j} Y_i^k \tag{21}$$

As it is easy to work out the shape function derivatives and the node coordinates are known, with eqs. (3), (4) and (6) the values of $\boldsymbol{L}$ and $\boldsymbol{S}$ can be worked out, followed by $\vec{g}$ and $\boldsymbol{H}$ through eqs. (14) and (16). The integrals over volume V_0 are performed numerically. For the triangular domain in ξ_1, ξ_2 Hammer quadrature is adopted, and Gauss-Legendre quadrature is used for the height domain in ξ_3. It can be worked out that for cubic functions Gauss-Legendre quadrature yields an exact integration result with only 2 points, whereas upon testing 12 Hammer integration points across the triangular base have shown to be sufficient.

2.2 Rectangular element for the steel decking and immersion technique

The degree of approximation of the rectangular elements must match that of the faces of the prismatic matrix element so there is node coincidence. Therefore, a 16-node element with cubic approximation in both directions is developed in a domain of variables $\bar{\xi}_1, \bar{\xi}_2$. Its geometry is approximated by a product of Lagrange polynomials, one for each of the plane directions. In $\bar{\xi}_3$ which is the direction normal to the element the thickness is assumed to be constant.

It must be noted that the bidimensional axes that define the rectangle's plane do not necessarily coincide with the global directions x_i, y_i. Thus, a local system $\bar{x}_i, \bar{y}_i$ must be defined. A rotation matrix that transits between the global and local systems is defined by

$$\boldsymbol{R} = \begin{bmatrix} \hat{u}_1 & \hat{u}_2 & \hat{u}_3 \\ \hat{v}_1 & \hat{v}_2 & \hat{v}_3 \\ \hat{w}_1 & \hat{w}_2 & \hat{w}_3 \end{bmatrix} \tag{22}$$

where $\hat{u}$ and $\hat{v}$ are versors that point to adimensional directions $\xi 1$ and ξ_2 of the element respectively and $\hat{w}$ is a versor normal to the plane (worked out by $\hat{u} \times \hat{v}$), as illustrated in Fig. 2.

The nodal coordinates must be first converted to the local system, which is done as follows:

$$\bar{X_i^k} = R_{ij} X_j^k \tag{23}$$

$$\bar{Y_i^k} = R_{ij} Y_j^k \tag{24}$$

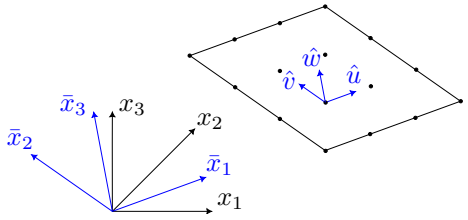

Figure 3. Rectangular element in global and local coordinate systems

Calculations are then carried out trough eqs. (20), (21), (3), (4) and (6) and local mechanical unbalanced force vector $\vec{\bar{g}}$ and Hessian matrix $\bar{\boldsymbol{H}}$ are worked out through eqs. (14) and (16). Plane strain state is assumed and the Poisson effect is ignored in the thickness direction, so no strains or stresses occur outside the plane and all calculations can be carried out in only 2 dimensions. The integral over volume V_0 yields the thickness value itself in $\bar{\xi}_3$ and can be performed numerically with two Gauss-Legendre quadratures for each of the directions $\bar{\xi}_1$ and $\bar{\xi}_2$.

The entities $\vec{\bar{g}}$ and $\bar{\boldsymbol{H}}$ must then be rotated back to the global system so they can contribute to the matrix element. The contribution is carried out for each matrix node that belongs to the active face region as shown below:

$$\vec{g} \leftarrow \vec{g} + \boldsymbol{R}^T \vec{\bar{g}} \tag{25}$$

$$\boldsymbol{H} \leftarrow \boldsymbol{H} + \boldsymbol{R}^T \bar{\boldsymbol{H}} \boldsymbol{R} \tag{26}$$

3 Validation examples

Two validation examples are presented below. The first one tests the behavior of immersed active face through a simple example reproductible by lienar elasticy, and the second one applies the current theory to a real steel deck beam.

3.1 Clamped beam with reinforcement plates

A 100 × 50 × 10 (length × width × height) clamped-free beam is subjected to a load distributed across its length of $q = -10^{-4}$. The beam matrix has Young modulus $E = 1$ and the top and bottom faces are stiffened with plates of Young modulus $E = 100$ and thickness $t = 0.1$. Through linear elasticy one can work out the maximum deflection on the free edge as $w = qL^4/8(EI)_{eq.}$, which in this case turns out to be $w = -0.0429$.

A 96 element mesh representing this problem yielded edge deflection value of $w = -0,0488$ which is only 4.72% apart from the linear elasticy results. The deformed mesh as well as the face elements are shown in Fig. 4.

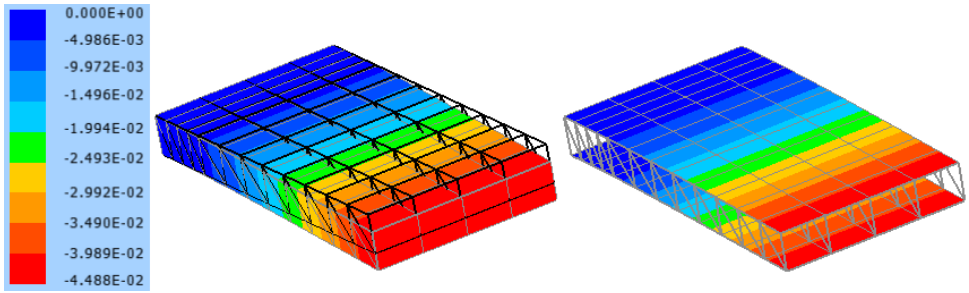

Figure 4. Clamped beam mesh and active face elements

3.2 Steeldeck beam under four point flexural test

Two meshes have been proposed to emulate a steel deck experiment ran by Gholamhoseini et al. [4]. The slab has been loaded to failure and cracking and slipping were observed, so only the initial window of linear behavior was selected for comparison.

Four-point flexural tests, see Fig. 5, were ran on concrete beams stiffened by a wave-form profile KF-70 manufactured by Fielders Australia Pty Ltd. [8], see Fig. 6. The nominal thickness and experimentally gauged Young modulus of the steel profiles were t = 0.075 cm and E_s = 212 GPa.

Figure 5. Experimental test setup

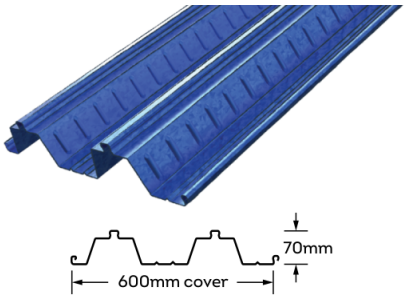

Figure 6. KF-70 steel decking profile

The beams were made to be 15 cm tall and the transverse sections made of 2 adjacent steel profiles each spanned 120 cm. The effective length of the structures was of 310 cm with extra 10 cm beyond the supports on each side. The Young modulus of the concrete was experimentally verified to be E_c = 30.725 GPa.

Two flexural tests were performed with loads applied at distances $L/4$ (ST70-4) and $L/6$ (ST70-6) from the supports.

To evaluate the effect of different levels of discretization, two cross section meshes, see Fig. 7, were generated and then extruded in 18 groups of elements across the length. The cross section shape was simplified as trapezoids and active face elements were included across all bottom faces of the mesh to represent the steel decking. The forces were applied on the top faces of the beam in steps of 5 kN as distributed loads across the entire width and in 5 cm strips across the length as to represent the spreader beams used in the experiments.

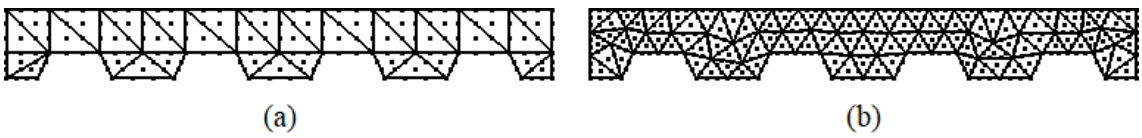

Figure 7. Transverse section meshes

In Fig. 8 the mid-span deflection results obtained by the present simulations are compared to the reference values.

4 Conclusions

The simulation of the clamped beam in 3.1 validates the proper behavior of the implementation as well as the stiffness contribution of the immersed active face element.

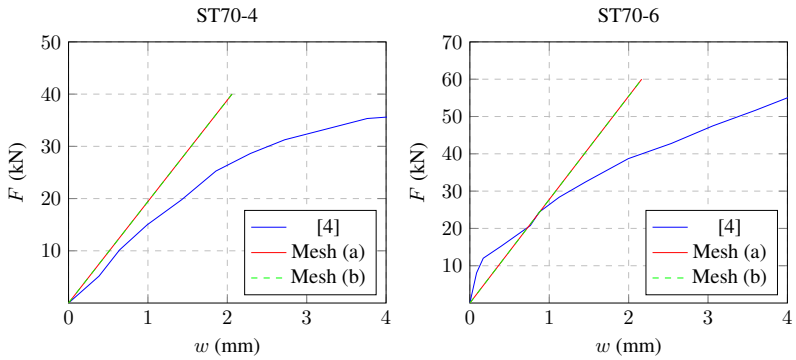

Figure 8. Mid-span deflection versus applied load

Regarding 3.2, it is easily noticeable in Fig. 8 that the simulated deflection behavior was fully linear, which outlines that geometrical nonlinearity was not a factor for the given loads. This leaves phenomena that the current theory does not encompass, such as layer slipping and cracking of the concrete, as the culprits of the nonlinearity of the experimental curves.

The heavier discretization of cross section mesh (a) into mesh (b) yielded no difference in the results, showing that the immersion of active faces has the same general effect on the structure even if the matrix elements are relatively big. This allows for less discrete and therefore lighter meshes to be used without any loss for this theory.

The relatively high difference between the experimental and simulated curves even on the linear region, notably on the ST70-6 case, could be explained by a number of factors. Even though the materials that constitute the beams had their properties tested, the fact only a single experiment was ran for each configuration may have brought uncertainties. On the simulation's side, the simplification of the decking's profile leading to the absence of the re-entrant bits may have had an impact in the resulting stiffness of the structure.

Nevertheless, with further studying so the material properties are properly calibrated and the mesh geometry is sufficiently descriptive of the analyzed problem, the present theory remains as a potential computationally lightweight candidate for quick evaluation of slabs under service loads.

Acknowledgements. This study was financed in part by the Coordenação de Aperfeiçoamento de Pessoal de Nível Superior - Brasil (CAPES) - Finance Code 001 - Process Number 88887.840098/2023-00, and by Brazilian National Council for Scientific and Technological Development (CNPq 302885/2022).

Authorship statement. The authors hereby confirm that they are the sole liable persons responsible for the authorship of this work, and that all material that has been herein included as part of the present paper is either the property (and authorship) of the authors, or has the permission of the owners to be included here.

References

[1] M. Patrick and R. Q. Bridge. Partial shear connection design of composite slabs. *Engineering Structures*, vol. 16, pp. 348–362, 1994.

[2] H.-Y. Kim and Y.-J. Jeong. Ultimate strength of a steel–concrete composite bridge deck slab with profiled sheeting. *Engineering Structures*, vol. 32, pp. 534–546, 2010.

[3] S. Chen and X. Shi. Shear bond mechanism of composite slabs — a universal fe approach. *Journal of Constructional Steel Research*, vol. 67, pp. 1475–1484, 2011.

[4] A. Gholamhoseini, R. Gilbert, M. Bradford, and Z. Chang. Longitudinal shear stress and bond–slip relationships in composite concrete slabs. *Engineering Structures*, vol. 69, pp. 37–48, 2014.

[5] J. Bonet, R. D. Wood, J. Mahaney, and P. Heywood. Finite element analysis of air supported membrane structures. *Computer Methods in Applied Mechanics and Engineering*, vol. 190, pp. 579–595, 2000.

[6] H. B. Coda and M. Greco. A simple fem formulation for large deflection 2d frame analysis based on position description. *Computer Methods in Applied Mechanics and Engineering*, vol. 193, pp. 3541–3557, 2004.

[7] R. Carrazedo, R. R. Paccola, and H. B. Coda. Active face prismatic positional finite element for linear and geometrically nonlinear analysis of honeycomb sandwich plates and shells. *Composite Structures*, vol. 200, pp. 849–863, 2018.

[8] *Specifying Fielders: KingFloor® Design Manual*. Fielders Australia Pty. Ltd., 2008.